Slight Multielement Doping-Induced Structural Order-Disorder Transition for High-Performance Layered Na-Ion Oxide Cathodes

Guo, Hao; Zhao, Chenglong; Gao, Jianxiang; Yang, Wenyun; Hu, Xufeng; Ma, Xiaobai; Jiao, Xuesheng; Yang, Jinbo; Sun, Kai; Chen, Dongfeng

DOI
10.1021/acsami.3c04843

Publication date
2023

Document Version
Final published version

Published in
ACS Applied Materials and Interfaces

ACS APPLIED MATERIALS & INTERFACES

www.acsami.org

Research Article

Slight Multielement Doping-Induced Structural Order−Disorder Transition for High-Performance Layered Na-Ion Oxide Cathodes

Hao Guo,* Chenglong Zhao,* Jianxiang Gao, Wenyun Yang, Xufeng Hu, Xiaobai Ma, Xuesheng Jiao, Jinbo Yang, Kai Sun,* and Dongfeng Chen*

Cite This: *ACS Appl. Mater. Interfaces* 2023, 15, 34789−34796

Read Online

ACCESS | Metrics & More | Article Recommendations | Supporting Information

ABSTRACT: To realize concurrently the high-energy density and excellent cycling stability, maximum utilization of redox couple, minimization of detrimental phase transition, and structural degradation of O3-type layered oxide cathodes are critical for developing Na-ion batteries. Ni^{2+}/Ni^{4+} redox couple showing multielectron reaction and higher redox potential is favorable to increase the energy density. However, the Jahn-Teller distortion of Ni^{3+} generated upon (dis)charging results in a strong anisotropy in the local crystal structure that causes irreversible interlayer bending and chemo-mechanical cracks of the cathode particles, compromising the electrochemical properties eventually. In this work, we show a slight multielement doping strategy that enlarges the amount of active redox components while minimizing the inactive contents. The results show that the uniform distribution of multiple components can help increase the disorder degree of atom arrangement and alleviate the structural changes and detrimental anisotropy cracks. As a proof of concept, a multielement-doped O3-type $Na_{0.9}Ni_{0.25}Cu_{0.05}Mg_{0.05}Zn_{0.05}Fe_{0.05}Al_{0.05}Mn_{0.40}Ti_{0.05}Sn_{0.05}O_2$ oxide is rationally prepared that presents better chemo-mechanical stability and delayed O3-P3 phase transition behavior. Compared to the high Ni-content $Na_{0.9}Ni_{0.35}Fe_{0.2}Mn_{0.45}O_2$ cathode, this as-prepared multielement material delivers a reversible capacity of about 120 mAh/g in the voltage range of 2−4.0 V, superior cycling stability with 90% of capacity retention after 500 cycles, and excellent rate capability (more than 70% of initial capacity at 5.0 C). This work indicates that the multielement doping method is highly suitable for the development of advanced Na-ion layered oxide cathodes.

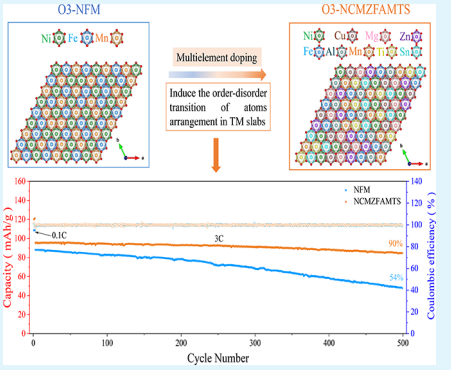

KEYWORDS: *multielement doping, order−disorder transition, anisotropy lattice strain, O3-type, $Na_{0.9}Ni_{0.25}Cu_{0.05}Mg_{0.05}Zn_{0.05}Fe_{0.05}Al_{0.05}Mn_{0.40}Ti_{0.05}Sn_{0.05}O_2$*

1. INTRODUCTION

Sodium-ion batteries (SIBs) are a promising alternative to Li-ion batteries (LIBs) in large-scale energy-storage systems due to the abundant sodium resources and low cost.[1−4] The performances of sodium-ion batteries such as energy density, cycling life, and fast charge ability are largely decided by cathode materials.[5−8] Considerable efforts in both engineering and scientific points of view have been devoted to exploring cathode materials with high reversible capacity, excellent cycling stability, and rate capability in the last decades.[9−13] Among the previously reported various cathode materials, Na-ion layered oxide (Na_xTMO_2, TM = transition metal) is one of most promising cathode materials for SIBs because of the easy preparation process and high theoretical capacity.[14−16]

According to Delmas' notation on layered oxides,[17] Na-ion layered oxides can be classified into two main groups, including O3-type and P2-type, where Na^+ occupies the octahedral (O) or prismatic (P) environment, respectively. The figures in two descriptions indicate that in a crystal cell, the numbers of TM layers along the stacking direction are 3 and 2, respectively. Generally, a high Na content ($x > 0.8$) enables the formation of a O3-type structure,[18] while the P2-type structure has a low Na content ($x < 0.7$).[19] In general, the P2-type layered oxides are likely to be affected by Na^+/vacancy ordering and structure transition during the charge and discharge process, which can be relieved by adjusting the compositions of Na sites and TM sites.[20,21] Compared with P2-type layered oxides, O3-type layered oxides have sufficient Na content and high initial capacity, which benefit the application of SIBs with high energy density. However, Na ions with large radius generally results in weak interlayer bonding for Na-ion layered oxides, which easily cause the gliding of the TMO_2 slabs upon desodiation.[22] This will lead to the formation of complicated phase transition in the layered cathodes. For example, O3-type $NaNi_{0.5}Mn_{0.5}O_2$ exhibits multiple phase transformations (O3−O'3−P3−P'3−

Received: April 5, 2023
Accepted: July 3, 2023
Published: July 13, 2023

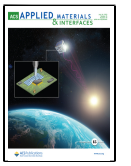

https://doi.org/10.1021/acsami.3c04843
ACS Appl. Mater. Interfaces 2023, 15, 34789−34796

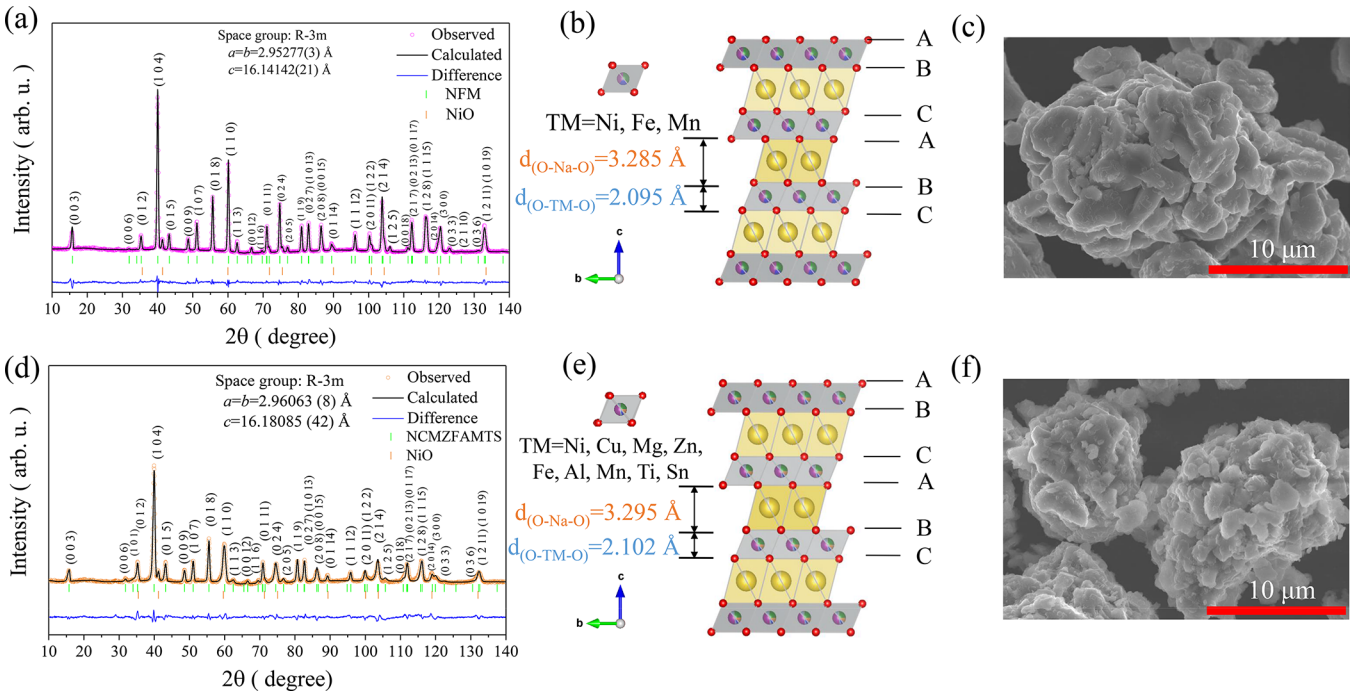

Figure 1. Crystal structure and morphology of NFM and NCMZFAMTS materials. NPD patterns and Rietveld refinement of NFM (a) and NCMZFAMTS (d). Schematic diagram of the crystal structure of NFM (b) and NCMZFAMTS (e). Morphology of NFM (c) and NCMZFAMTS (f).

P3") during the charge−discharge processes, which have a detrimental influence on the electrochemical performance.[23] The pioneering works have proven that the rational component design can suppress the phase transition of O3-Na_xTMO_2 cathodes and facilitate reversible O3−P3 phase transition, thereby improving the electrochemical properties.[24−26] In addition, the anisotropic lattice strain generated upon (dis)charging, which primarily results from the intrinsic evolution of anisotropic lattice parameters, can usually cause structural degradation including the formation of cracks.[27] This structural degradation is more severe in the case of Ni-rich oxides. Some feasible strategies including specific elemental doping,[28] microstructure engineering,[29] and single-crystal development[30] have been proposed to mitigate the structural degradations resulting from the anisotropic lattice strain. Recently, high-entropy (HE) materials have attracted more attention for their improved comprehensive performance attributed to the increasing entropy by multiple elements occupying simultaneously on the same lattice sites, which provide new perspectives for designing high-performance functional materials.[31−33] The HE strategy has managed to introduce Na-ion layered oxides, which demonstrates the delayed O3 to P3 phase transition, contributing to improved cycling stability. However, equimolar mixtures of active and inactive TMs result in a limited capacity due to invalid redox couples.[32]

In this work, we report a new HE method of doping multiple active and inactive elements in slight concentration, which enables the design of higher-performance O3-type Na-ion layered cathodes. First, the multiple active elements involving redox can provide enough capacity; second, doping slightly multiple active and inactive elements that occupy the equivalent lattice positions helps to increase the disorder degree of atom arrangement in TM slabs and results in the order−disorder transition of active elements, which can dilute anisotropic lattice strain upon (dis)charging. Meanwhile, slightly multiple inactive element in the crystal structure can serve as rivets to increase the robustness of the structure and mitigate the harmful effect originated from anisotropic lattice strain,[27] thereby promoting excellent chemo-mechanical stability and cycling performance. The slight multielement doped $Na_{0.9}Ni_{0.25}Cu_{0.05}Mg_{0.05}Zn_{0.05}Fe_{0.05}Al_{0.05}Mn_{0.40}Ti_{0.05}Sn_{0.05}O_2$ material (denoted here as NCMZFAMTS) shows a delayed O3-P3 phase transition behavior without the appearance of Na^+/vacancy and distortion phase transition and better chemo-mechanical stability than the control O3-type $Na_{0.9}Ni_{0.35}Fe_{0.2}Mn_{0.45}O_2$ (denoted here as NFM) material. Consequently, the NCMZFAMTS cathode shows exceptional comprehensive performance including excellent cycling stability and rate capability.

2. EXPERIMENTAL SECTION

2.1. Material Preparation. $Na_{0.9}Ni_{0.25}Cu_{0.05}Mg_{0.05}Zn_{0.05}Fe_{0.05}Al_{0.05}Mn_{0.40}Ti_{0.05}Sn_{0.05}O_2$ (NCMZFAMTS) and $Na_{0.9}Ni_{0.35}Fe_{0.20}Mn_{0.45}O_2$ (NFM) samples were prepared by a high-temperature solid-state reaction using Na_2CO_3 (99%), NiO (99%), ZnO (99%), MgO (99%), CuO (99%), Fe_2O_3 (99%), Al_2O_3 (99%), MnO_2 (98%), TiO_2 (99%), and SnO_2 (99%) as precursors. An excess of 2 mol % Na_2CO_3 was used. The precursors were adequately mixed and ground and then pressed into pellets with a diameter of 12 mm. The obtained pellets were sintered at 950 °C under air with a heating rate of 5 °C/min, held at 950 °C for 15 h, and cooled to room temperature naturally.

2.2. Structure Characterization. Inductively coupled plasma-atomic emission spectroscopy (ICP-AES, Agilent, ICPOES730) was used to analyze the chemical compositions of the obtained materials. X-ray diffraction (XRD) experiments were performed on a D8 Bruker X-ray diffractometer using Cu Kα radiation (λ_1 = 1.54060 Å, λ_2 = 1.54439 Å). Neutron powder diffraction (NPD) patterns were collected by using at high-intensity powder diffractometer at the China advanced research reactor of China Institute of Atomic Energy.

https://doi.org/10.1021/acsami.3c04843
ACS Appl. Mater. Interfaces 2023, 15, 34789−34796

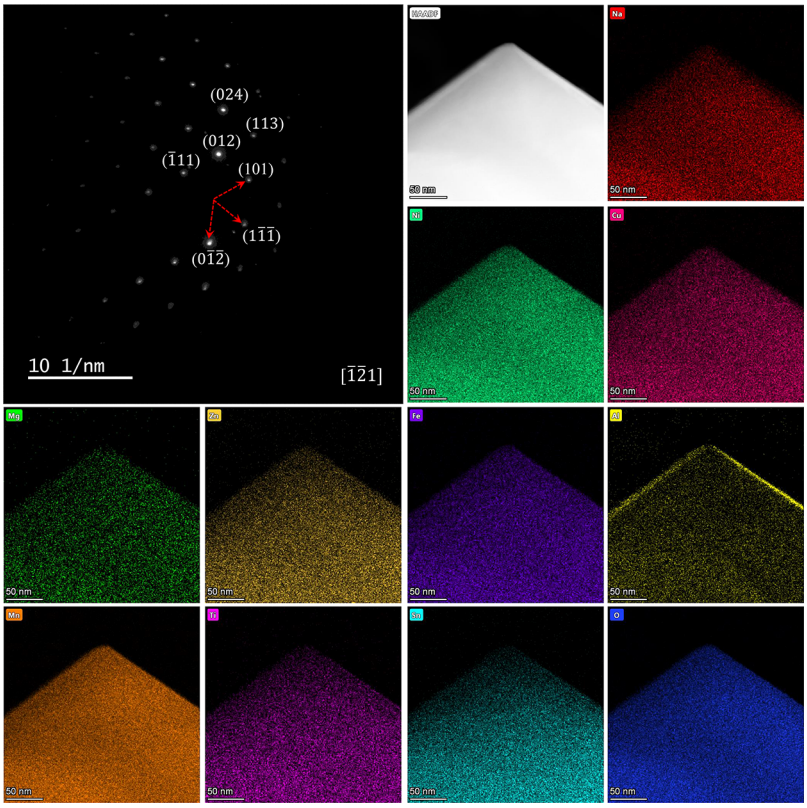

Figure 2. Selected area electron diffraction result and EDS mappings of the O3-type NCMZFAMTS sample.

The wavelength used was 1.4798 Å. The XRD and NPD data were refined by using the Rietveld method. Microstructure of NCMZFAMTS and NFM samples, including morphology, particle size, and element distribution, were characterized by scanning electron microscopy (SEM, Regulus-8100) and high-resolution transmission electron microscopy (HRTEM, JEM-F200).

2.3. Electrochemical Measurements. The electrodes taking part in testing were prepared by rolling the mixture of active materials (80 wt %), carbon nanotubes (15 wt %), and polytetrafluoroethylene (5 wt %) into thin films with the loading mass of ∼5 mg/cm^2. The electrochemical properties were tested in CR-2032 coin cells, which were assembled using Na foil as the counter electrode and a glass fiber as the separator in an argon-filled glovebox. The electrolyte used was 1.0 M $NaClO_4$/propylene carbonate/ethylene carbonate (1:1 in volume) with 5% fluoroethylene carbonate. The galvanostatic charge−discharge measurements of cells were performed on a Neware battery cycler (CT-4008T, Shenzhen, China) test system. A CHI660E Electrochemical Workbench (Shanghai, China) was used for cyclic voltammetry (CV) scanning. A Swagelok cell equipped with an Al window was used for the in situ measurements upon charge and discharge. For the ex-situ SEM experiments, the electrodes were cycled in the voltage range of 2−4 V at 1C rate. After 300 cycles, the electrodes were disassembled to collect the cathodes in an Ar-filled glovebox and washed with dimethyl carbonate.

3. RESULTS AND DISCUSSION

3.1. Crystal Structural Analysis. NCMZFAMTS and NFM samples were obtained by a high-temperature calcination process, as described in the Experimental Section. As shown in Figure S1, the XRD results indicate that the diffraction peaks of two samples are consistent with those of O3-type $Na_{0.9}Ni_{0.45}Ti_{0.55}O_2$ (JCPDS No. 96-152-6611), except a few NiO impurities. To study the detailed phase structure and phase ratio, we conducted NPD measurements. As displayed in Figure 1a,d, the Rietveld refinement of NPD data indicates that the diffraction peaks of two samples can be well indexed with the *R*-3*m* space group. The corresponding crystal structures, depicted in Figure 1b,e, are built up by edge-sharing [TMO_6] octahedra, forming repeating ABCABC arrangements of oxygen stacking between which Na ions are occupied in the octahedral environments of the O3-type layered structure. The obtained cell parameters, atomic occupancies, and isotropic displacement parameters of O3-NFM and O3-NCMZFAMTS materials are displayed in Tables S1 and S2. It can be found that the lattice parameter *c* and the $d_{(O-TM-O)}$ interlayer distance of NCMZFAMTS (c = 16.181 Å, $d_{(O-TM-O)}$ = 2.102 Å) increase significantly compared with those of NFM (c = 16.141 Å, $d_{(O-TM-O)}$ = 2.095 Å), indicating that these doped elements successfully incorporate into the crystal lattice. In addition, we analyzed the variation of (110) diffraction peaks of both samples. It can be seen from Figure S2 that the (110) peak of NCMZFAMTS shows an obvious broadening compared with that of NFM. This is attributed to the fluctuation of interplanar spacing of the (110) plane resulting from the same lattice sites occupied simultaneously by different elements. Therefore, the broadening of the (110) peak indicates that the atom arrangement in TM sites becomes more disordered. The effect of order−disorder transition on the structure and performance of cathodes will be discussed later. ICP-AES results indicate that the overall compositions of the two materials are consistent with the designed components (Table S3) and the results obtained by NPD, demonstrating the feasibility of multielement doping. SEM was used to observe the morphology of as-prepared samples. Results show that the particles of both samples have a blocky-shaped morphology with the size distribution of 2−10 μm (Figures 1c,f and S3).

https://doi.org/10.1021/acsami.3c04843
ACS Appl. Mater. Interfaces 2023, 15, 34789−34796

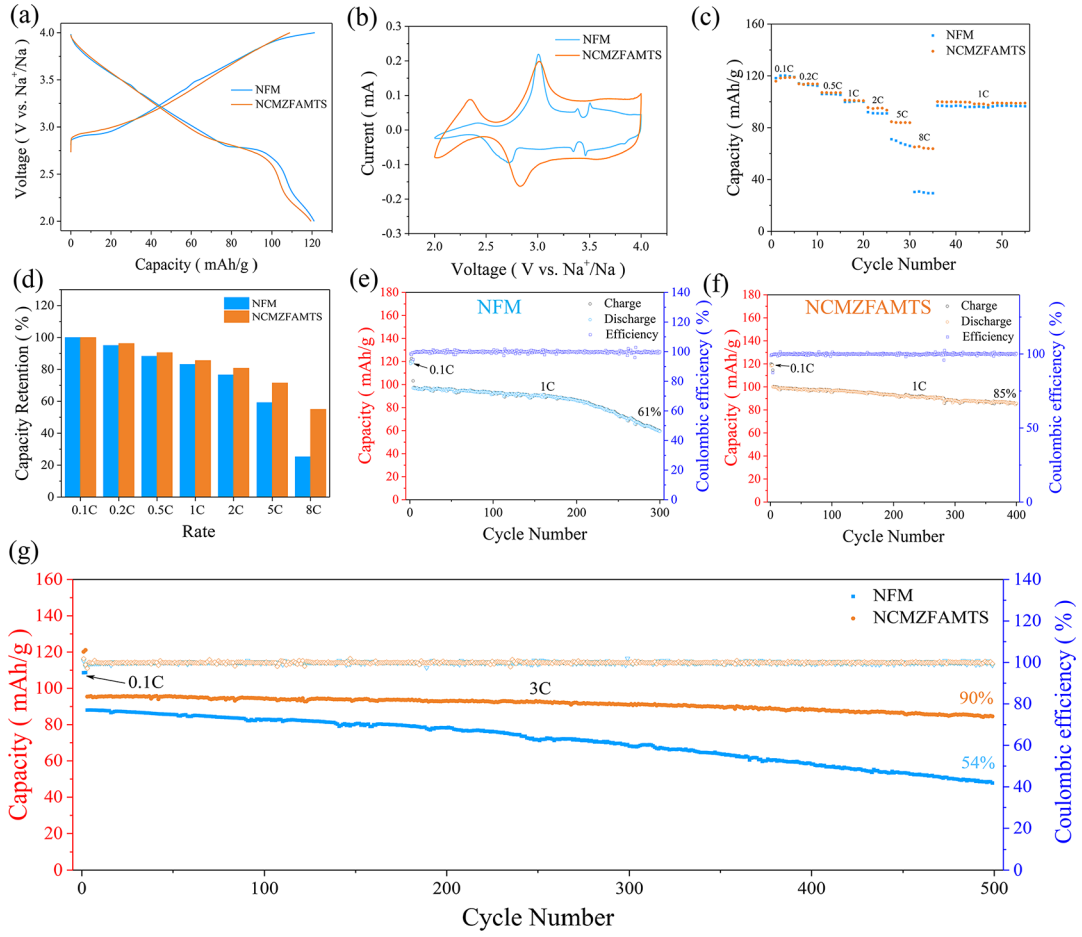

Figure 3. Electrochemical properties of NFM and NCMZFAMTS cathodes. (a)First charge−discharge curves of NFM and NCMZFAMTS cathodes at 0.1 C between 2.0 and 4.0 V. (b) CV profiles of NFM and NCMZFAMTS cathodes scanned between 2.0 and 4.0 V at a rate of 0.1 mV/s. (c) Rate capability and (d) capacity retention ratios when both the cathodes were cycled at 0.1, 0.2, 0.5, 1, 2, 5, and 8 C. (e−g) Cycling performance at 1 and 3C rates.

The detailed microstructure of the NCMZFAMTS sample is also investigated by HRTEM. As presented in Figure 2, the diffraction spots can be well matched with the (101) and (012) planes for O3-NCMZFAMTS, compatible with the results of NPD refinement. In addition, it can be seen from energy-dispersive X-ray spectroscopy (EDS) elementary mapping images that Na, Ni, Cu, Mg, Zn, Fe, Al, Mn, Ti, Sn, and O elements of the as-prepared sample are uniformly distributed except for the slight surface enrichment of Al, suggesting further the practicability of the multielement doping method.

3.2. Electrochemical Performance. To investigate the positive effect of the multielement doping method on the performance of materials, we conducted charge and discharge testing for the O3-type NFM and NCMZFAMTS electrodes by using coin-type half cells with a Na metal anode. As shown in Figures 3a and S4a, the O3-NCMZFAMTS cathode delivers a reversible capacity of approximately 120 mAh g^{-1} in the voltage range of 2.0−4.0 V at 0.1C (12 mA g^{-1}), higher than that of the previously reported HE O3-type cathode.[32,34] Accordingly, the O3-NFM cathode shows a similar reversible capacity of 122 mAh g^{-1} in the same condition. Significantly, this HE NCMZFAMTS cathode has less active redox couple than NFM, but both cathodes show a similar capacity, which highlights the feasibility of multielement doping in O3-NCMZFAMTS. In addition, in the CV profiles of Figures 3b and S4b, the NFM cathode shows anodic/cathodic peaks at about 3.02/2.72 V and small humps at 3.45/3.40 V, which are consistent with the obvious and quasi voltage plateaus in charge and discharge curves, respectively. The latter can be attributed to the Na^+/vacancies order−disorder transition.[35] However, a noticeable phenomenon is that the specific humps and the quasi voltage plateau are absent in the case of the NCMZFAMTS electrode, and the intensities of anodic/cathodic peaks at about 3.06/2.78 V for NCMZFAMTS are weaker than those of the NFM electrode. This phenomenon could be attributed to the changed phase transition process induced by slight multielement doping. The difference in charge−discharge curves and CV profiles between NFM and NCMZFAMTS electrodes indicates that the multielement doping strategy has a significant effect on the Na-storage performance. To evaluate this effect in detail, we conducted the rate performance and cycling stability tests of both cathodes. As presented in Figures 3c,d and S4, the reversible capacities of the NCMZFAMTS electrode are about 118, 114, 107, 101, 96, 85, and 65 mAh/g at rates of 0.1, 0.2, 0.5, 1, 2, 5, and 8 C, respectively. As for NFM, the reversible capacities at the same rates are about 121, 114, 106, 100, 92, 71, and 30 mAh/g. Although the NCMZFAMTS electrode shows a slightly low capacity at 0.1 C than NFM, the capacity retentions of multicomponent-doped NCMZFAMTS are evidently higher than those of undoped NFM, especially at high rates, demonstrating the improved rate capability (more

https://doi.org/10.1021/acsami.3c04843
ACS Appl. Mater. Interfaces 2023, 15, 34789−34796

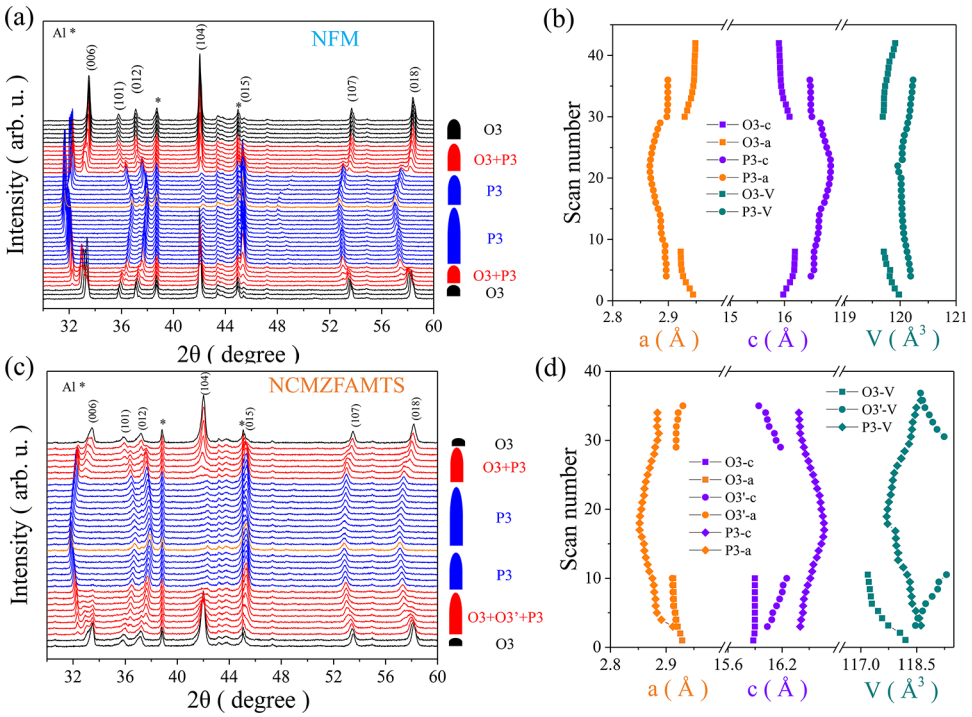

Figure 4. Structural evolution upon charging and discharging. In situ XRD patterns of NFM (a) and NCMZFAMTS (c) electrodes during the first charge/discharge course in the voltage range of 2−4 V, respectively. Cell parameter evolution of NFM (b) and NCMZFAMTS (d) electrodes during the first charge/discharge cycle.

than 70% of initial capacity at 5 C). This can be rationally implied by the increased D_{Na^+} of NCMZFAMTS than that of NFM obtained by the galvanostatic intermittent titration technique (GITT) measurements. It can be seen from Figure S5 that D_{Na^+} of the NCMZFAMTS cathode stabilizes at 10^{-10}−10^{-11} cm^2/s, which is almost twice as much as that of the NFM cathode.

Most importantly, the NCMZFAMTS cathode shows much improved long-term cycling performance at different current densities (Figure 3e−g). Typically, when cycled in a voltage range of 2.0−4.0 V at 3C rate, NFM displays rapid capacity degradation (capacity retention of 54%). By contrast, NCMZFAMTS shows a much more excellent cycling stability with the capacity conservation rate of 90% after 500 cycles, which is also better than those of previously reported O3-type cathodes (Table S4). It should be mentioned that some HE O3-type cathodes can deliver higher capacity when cycled in a wider voltage range but at the expense of the cycling performance. For example, under the voltage window of 2.0−4.5 V, the O3-$Na_{2/3}Li_{1/6}Fe_{1/6}Co_{1/6}Ni_{1/6}Mn_{1/3}O_2$ cathode delivers a capacity of 171 mAh/g but suffers from the fast capacity decay (89.3% capacity retention at 1 C for 90 cycles).[36] Therefore, the excellent rate capabilities and superior cycle stability prove that the O3-type NCMZFAMTS cathode is a promising cathode for SIBs with a long operation life.

3.3. Structural Evolution upon Charging and Discharging. To explain the performance enhancement mechanism, we performed in-situ XRD measurements to investigate the structural evolution of NFM and NCMZFAMTS electrodes during the first charge/discharge process. As demonstrated in Figures 4a and S6a, when charging started, the (006) diffraction peak of the NFM electrode shifted gradually to a lower 2θ angle, while the (101) peak shifted to a higher 2θ angle, indicating the expansion of the interlayer distance and shrinkage of interplanar distance (cell parameters c and a in Figure 4b), respectively. These contrary changes of cell parameters (a and c) result in a decrease in the cell volume.[37] Upon further charging, a new (006) peak emerged at a lower angle, and the peak intensity increased gradually, demonstrating the occurrence of O3−P3 phase transformation. Then, the peaks of the O3 structure disappear, and only those of the P3 structure remain in the XRD pattern. With charging until to 4 V, the (006) peak of the P3 phase shifts continuously to a lower angle, demonstrating a solid-solution reaction. During the subsequent discharge course, the NFM electrode presented a opposite phase evolution and transformed back to a single O3 phase. In the case of multielement-doped NCMZFAMTS, it can be seen from Figures 4c and S6 that NCMZFAMTS displays an obviously different phase transition behavior compared with NFM. Upon charging, the intensity of the (006) peak belonging to the O3 phase decreased gradually, and two new (006) peaks emerged at a lower angle. It is noteworthy that (20−2) and (111) peaks of the monoclinic O'3 phase are absent around the (104) peak. Therefore, it is reasonable to think that new O3' (another O3 structure with different cell parameters) and P3 phases appear, suggesting that O3-type NCMZFAMTS does not directly transform to the P3 phase but goes through a three-phase mixing course. Upon further charging, the peaks of O3 and O3' phases completely disappear, and P3 phase keeps a solid-solution reaction until charged to 4 V without the appearance of any new phase. In the following discharge course, the P3 phase transforms back to the O3' phase by the two-phase course, demonstrating a different phase transition behavior compared with the charge course.

3.4. Mechanism of Modification. O3-type Na-ion layered oxides are prone to degradation under electrochemical cycling, which is related to structural degradation, phase

https://doi.org/10.1021/acsami.3c04843
ACS Appl. Mater. Interfaces 2023, 15, 34789−34796

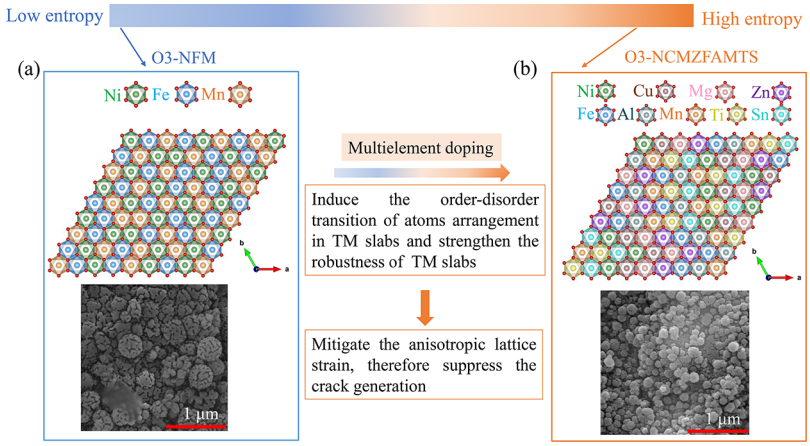

Figure 5. Mechanism of the slight multielement doping strategy for layered oxides. (a) typical O3-type Na-ion layered oxides such as NFM. (b) Multielement-doped O3-type HE oxide such as NCMZFAMTS. The upper parts in Figure 5a,b present the TMO_6 octahedron arrangement in 9a × 9a superlattice of NFM and NCMZFAMTS, respectively. The lower parts show SEM pictures of NFM and NCMZFAMTS electrodes after 300 cycles at 1 C rate.

transition, and surface reconstruction of the electrode particles.[38] The larger Na^+ (vs TMs) and strong Na^+−Na^+ electrostatic repulsion in NaO_2 slabs result in complicated phase transition upon (de)sodiation.[39] Recent research shows that the increasing entropy stabilizing the host matrix facilitates the layered O3-type structure to a larger extent, which results in $NaNi_{0.12}Cu_{0.12}Mg_{0.12}Fe_{0.15}Co_{0.15}Mn_{0.1}Ti_{0.1}Sn_{0.1}Sb_{0.04}O_2$ cathode demonstrating delayed O3 to P3 transition that manifests as a longer voltage plateau in the charge−discharge curves.[32] In the case of multielement-doped NCMZFAMTS cathode, this long voltage plateau in the charge−discharge curves is absent; instead, the slope character becomes obvious, corresponding to a three-phase mixing course (O3−O3'−P3). This particular and delayed O3−P3 phase transition process contributes to excellent cycling stability.

Multielectron reaction of Ni^{2+}/Ni^{4+} redox couple, which serves as charge compensators to increase the energy density, is desirable for the cathodes. However, the Ni^{3+} Jahn-Teller distortion generated upon (dis)charging can result in a strong anisotropy of the local crystal structure. This strong anisotropy could cause irreversible interlayer bending and formation of multiple kinks that would accumulate with electrochemical cycling, eventually leading to chemo-mechanical cracking and performance degradation.[22,40] To explore the effect of multielement doping on the chemo-mechanical stability, we characterized the morphology evolution of NFM and NCMZFAMTS electrodes after 300 cycles. As shown in Figure 5, it can be clearly seen from SEM pictures that after 300 cycles at 1 C rate, cracks appear in almost all NFM particles, but those are absent in the case of NCMZFAMTS, which demonstrates that NCMZFAMTS has better chemo-mechanical stability than NFM. Based on the above results, we propose a possible mechanism to explain the enhancement mechanism of multielement doping strategy. The local structure of NFM is liable to be affected by Ni^{3+} with the Jahn-Teller distortion, which results in the weak stability of TM slabs. With electrochemical cycling, the weak TM slabs are prone to bending and slipping, and therefore many cracks are present in NFM particles and performance degradation occurs. By doping a variety of active and inert elements into TMO_2 slabs, on the one hand, the distance of the slabs can be enlarged, which can mitigate the expansion and contraction of active $[TMO_6]$ octahedrons; on the other hand, multielement doping will lead to discrete distribution of Ni in the structure matrix, complicated local interactions between TMs and Na, and robust TMO_2 slabs, which could relieve Jahn−Teller distortion of Ni^{3+}. This means that the increasing entropy by introducing more slight elements in the host structure can enable the order−disorder transition and strengthen the robustness of TMO_2 slabs, which reduce the phase transition, mitigate the anisotropic lattice strain, and suppress the cracking generation, leading to improved cycling stability.

4. CONCLUSIONS

In summary, we showed a slight multielement doping strategy that enlarged the variety of doped components and limited their contents and successfully prepared a HE O3-type $Na_{0.9}Ni_{0.25}Cu_{0.05}Mg_{0.05}Zn_{0.05}Fe_{0.05}Al_{0.05}Mn_{0.40}Ti_{0.05}Sn_{0.05}O_2$ material. The random distribution of multiple active and inactive elements results in the order−disorder transition of atom arrangement in TM slabs and strengthens their robustness, which can facilitate the delayed O3−P3 phase transition and suppress the cracking generation. Therefore, NCMZFAMTS cathode exhibits excellent chemo-mechanical stability and improved comprehensive performance. The proposed multielement doping strategy helps to realize concurrently the high energy density and excellent cycling stability and rate capability, which provides rational guidance for designing a high-performance layered Na-ion oxide cathode.

■ ASSOCIATED CONTENT

Supporting Information

The Supporting Information is available free of charge at https://pubs.acs.org/doi/10.1021/acsami.3c04843.

XRD patterns; illustration of TM layer and (110) crystal plane; atomic coordinates, occupancies, and isotropic displacement parameters obtained by refining NPD data; ICP results; EDS mappings of the NFM sample; CV curves and voltage profiles of NFM and NCMZFAMTS electrodes; electrochemical performance comparison of O3-type layered oxide cathodes; GITT curves and Na^+ diffusivity; and 2D contour plots of in situ XRD (PDF)

https://doi.org/10.1021/acsami.3c04843
ACS Appl. Mater. Interfaces 2023, 15, 34789−34796

AUTHOR INFORMATION

Corresponding Authors

Hao Guo − *China Institute of Atomic Energy, Beijing 102413, P. R. China*; orcid.org/0000-0003-1764-9589; Email: guohao@ciae.ac.cn

Chenglong Zhao − *Department of Radiation Science and Technology, Delft University of Technology, Delft 2629JB, Netherlands*; Email: c.zhao-1@tudelft.nl

Kai Sun − *China Institute of Atomic Energy, Beijing 102413, P. R. China*; Email: ksun@ciae.ac.cn

Dongfeng Chen − *China Institute of Atomic Energy, Beijing 102413, P. R. China*; Email: dongfeng@ciae.ac.cn

Authors

Jianxiang Gao − *China Institute of Atomic Energy, Beijing 102413, P. R. China*

Wenyun Yang − *State Key Laboratory for Mesoscopic Physics, School of Physics, Peking University, Beijing 100871, P. R. China*

Xufeng Hu − *China Institute of Atomic Energy, Beijing 102413, P. R. China*

Xiaobai Ma − *China Institute of Atomic Energy, Beijing 102413, P. R. China*

Xuesheng Jiao − *China Institute of Atomic Energy, Beijing 102413, P. R. China*

Jinbo Yang − *State Key Laboratory for Mesoscopic Physics, School of Physics, Peking University, Beijing 100871, P. R. China*; orcid.org/0000-0003-3517-9701

Complete contact information is available at: https://pubs.acs.org/10.1021/acsami.3c04843

Notes

The authors declare no competing financial interest.

ACKNOWLEDGMENTS

This work was financially supported by the National Natural Science Foundation of China (grant no. 12105372).

REFERENCES

(1) Sun, Y.; Shi, P.; Chen, J.; Wu, Q.; Liang, X.; Rui, X.; Xiang, H.; Yu, Y. Development and challenge of advanced nonaqueous sodium ion batteries. *EnergyChem* **2020**, *2*, No. 100031.

(2) Komaba, S. Sodium-driven Rechargeable Batteries: An Effort towards Future Energy Storage. *Chem. Lett.* **2020**, *49*, 1507−1516.

(3) Zhao, C.; Lu, Y.; Chen, L.; Hu, Y.-S. Flexible Na batteries. *InfoMat* **2020**, *2*, 126−138.

(4) Delmas, C. Sodium and Sodium-Ion Batteries: 50 Years of Research. *Adv. Energy Mater.* **2018**, *8*, No. 1703137.

(5) Huang, Y.; Zheng, Y.; Li, X.; Adams, F.; Luo, W.; Huang, Y.; Hu, L. Electrode Materials of Sodium-Ion Batteries toward Practical Application. *ACS Energy Lett.* **2018**, *3*, 1604−1612.

(6) Han, M. H.; Gonzalo, E.; Singh, G.; Rojo, T. A comprehensive review of sodium layered oxides: powerful cathodes for Na-ion batteries. *Energy Environ. Sci.* **2015**, *8*, 81−102.

(7) Liu, Y.; Wang, D.; Li, H.; Li, P.; Sun, Y.; Liu, Y.; Liu, Y.; Zhong, B.; Wu, Z.; Guo, X. Research progress in O3-type phase Fe/Mn/Cu-based layered cathode materials for sodium ion batteries. *J. Mater. Chem. A* **2022**, *10*, 3869−3888.

(8) Zhao, C.; Lu, Y.; Chen, L.; Hu, Y.-S. Ni-based cathode materials for Na-ion batteries. *Nano Res.* **2019**, *12*, 2018−2030.

(9) Rudola, A.; Rennie, A. J. R.; Heap, R.; Meysami, S. S.; Lowbridge, A.; Mazzali, F.; Sayers, R.; Wright, C. J.; Barker, J. Commercialisation of high energy density sodium-ion batteries: Faradion's journey and outlook. *J. Mater. Chem. A* **2021**, *9*, 8279−8302.

(10) Hu, Y.-S.; Li, Y. Unlocking Sustainable Na-Ion Batteries into Industry. *ACS Energy Lett.* **2021**, *6*, 4115−4117.

(11) Zhao, Y.; Liu, Q.; Zhao, X.; Mu, D.; Tan, G.; Li, L.; Chen, R.; Wu, F. Structure evolution of layered transition metal oxide cathode materials for Na-ion batteries: Issues, mechanism and strategies. *Mater. Today* **2023**, *62*, 271−295.

(12) Bianchini, M.; Xiao, P.; Wang, Y.; Ceder, G. Additional Sodium Insertion into Polyanionic Cathodes for Higher-Energy Na-Ion Batteries. *Adv. Energy Mater.* **2017**, *7*, No. 1700514.

(13) Wang, L.; Song, J.; Qiao, R.; Wray, L. A.; Hossain, M. A.; Chuang, Y.-D.; Yang, W.; Lu, Y.; Evans, D.; Lee, J.-J.; et al. Rhombohedral Prussian White as Cathode for Rechargeable Sodium-Ion Batteries. *J. Am. Chem. Soc.* **2015**, *137*, 2548−2554.

(14) Zhao, C.; Wang, Q.; Yao, Z.; Wang, J.; Sánchez-Lengeling, B.; Ding, F.; Qi, X.; Lu, Y.; Bai, X.; Li, B.; et al. Rational design of layered oxide materials for sodium-ion batteries. *Science* **2020**, *370*, 708.

(15) Delmas, C.; Carlier, D.; Guignard, M. The Layered Oxides in Lithium and Sodium-Ion Batteries: A Solid-State Chemistry Approach. *Adv. Energy Mater.* **2021**, *11*, No. 2001201.

(16) Kubota, K.; Yabuuchi, N.; Yoshida, H.; Dahbi, M.; Komaba, S. Layered oxides as positive electrode materials for Na-ion batteries. *MRS Bull.* **2014**, *39*, 416−422.

(17) Delmas, C.; Fouassier, C.; Hagenmuller, P. Structural classification and properties of the layered oxides. *Phys. B+C* **1980**, *99*, 81−85.

(18) Xiao, B.; Liu, X.; Song, M.; Yang, X.; Omenya, F.; Feng, S.; Sprenkle, V.; Amine, K.; Xu, G.; Li, X.; et al. A general strategy for batch development of high-performance and cost-effective sodium layered cathodes. *Nano Energy* **2021**, *89*, No. 106371.

(19) Vasavan, H. N.; Badole, M.; Dwivedi, S.; Kumar, D.; Kumar, P.; Kumar, S. Enhanced rate performance and specific capacity in Ti-substituted P2-type layered oxide enabled by crystal structure and particle morphology modifications. *Chem. Eng. J.* **2022**, *448*, No. 137662.

(20) Li, X.-L.; Wang, T.; Yuan, Y.; Yue, X.-Y.; Wang, Q.-C.; Wang, J.-Y.; Zhong, J.; Lin, R.-Q.; Yao, Y.; Wu, X.-J.; et al. Whole-Voltage-Range Oxygen Redox in P2-Layered Cathode Materials for Sodium-Ion Batteries. *Adv. Mater.* **2021**, *33*, No. 2008194.

(21) Wang, Q.-C.; Shadike, Z.; Li, X.-L.; Bao, J.; Qiu, Q.-Q.; Hu, E.; Bak, S.-M.; Xiao, X.; Ma, L.; Wu, X.-J.; et al. Tuning Sodium Occupancy Sites in P2-Layered Cathode Material for Enhancing Electrochemical Performance. *Adv. Energy Mater.* **2021**, *11*, No. 2003455.

(22) Li, Y.; Li, X.; Du, C.; Sun, H.; Zhang, Y.; Liu, Q.; Yang, T.; Zhao, J.; Delmas, C.; Harris, S. J.; et al. Degradation by Kinking in Layered Cathode Materials. *ACS Energy Lett.* **2021**, *6*, 3960−3969.

(23) Komaba, S.; Yabuuchi, N.; Nakayama, T.; Ogata, A.; Ishikawa, T.; Nakai, I. Study on the reversible electrode reaction of Na(1-x)Ni(0.5)Mn(0.5)O2 for a rechargeable sodium-ion battery. *Inorg. Chem.* **2012**, *51*, 6211−6220.

(24) Guo, H.; Avdeev, M.; Sun, K.; Ma, X.; Wang, H.; Hu, Y.; Chen, D. Pentanary transition-metals Na-ion layered oxide cathode with highly reversible O3-P3 phase transition. *Chem. Eng. J.* **2021**, *412*, No. 128704.

(25) Yao, H.-R.; Lv, W.-J.; Yin, Y.-X.; Ye, H.; Wu, X.-W.; Wang, Y.; Gong, Y.; Li, Q.; Yu, X.; Gu, L.; et al. Suppression of Monoclinic Phase Transitions of O3-Type Cathodes Based on Electronic Delocalization for Na-Ion Batteries. *ACS Appl. Mater. Interfaces* **2019**, *11*, 22067−22073.

(26) You, Y.; Xin, S.; Asl, H. Y.; Li, W.; Wang, P.-F.; Guo, Y.-G.; Manthiram, A. Insights into the Improved High-Voltage Performance of Li-Incorporated Layered Oxide Cathodes for Sodium-Ion Batteries. *Chem* **2018**, *4*, 2124−2139.

(27) Wang, L.; Liu, T.; Wu, T.; Lu, J. Strain-retardant coherent perovskite phase stabilized Ni-rich cathode. *Nature* **2022**, *611*, 61−67.

(28) Weigel, T.; Schipper, F.; Erickson, E. M.; Susai, F. A.; Markovsky, B.; Aurbach, D. Structural and Electrochemical Aspects of LiNi0.8Co0.1Mn0.1O2 Cathode Materials Doped by Various Cations. *ACS Energy Lett.* **2019**, *4*, 508−516.

(29) Yan, P.; Zheng, J.; Liu, J.; Wang, B.; Cheng, X.; Zhang, Y.; Sun, X.; Wang, C.; Zhang, J.-G. Tailoring grain boundary structures and chemistry of Ni-rich layered cathodes for enhanced cycle stability of lithium-ion batteries. *Nat. Energy* **2018**, *3*, 600−605.
(30) Langdon, J.; Manthiram, A. A perspective on single-crystal layered oxide cathodes for lithium-ion batteries. *Energy Storage Mater.* **2021**, *37*, 143−160.
(31) Zhang, R.; Wang, C.; Zou, P.; Lin, R.; Ma, L.; Yin, L.; Li, T.; Xu, W.; Jia, H.; Li, Q.; et al. Compositionally complex doping for zero-strain zero-cobalt layered cathodes. *Nature* **2022**, *610*, 67−73.
(32) Zhao, C.; Ding, F.; Lu, Y.; Chen, L.; Hu, Y.-S. High-Entropy Layered Oxide Cathodes for Sodium-Ion Batteries. *Angew. Chem., Int. Ed.* **2020**, *59*, 264−269.
(33) Sarkar, A.; Velasco, L.; Wang, D.; Wang, Q.; Talasila, G.; de Biasi, L.; Kübel, C.; Brezesinski, T.; Bhattacharya, S. S.; Hahn, H.; Breitung, B. High entropy oxides for reversible energy storage. *Nat. Commun.* **2018**, *9*, 3400.
(34) Tian, K.; He, H.; Li, X.; Wang, D.; Wang, Z.; Zheng, R.; Sun, H.; Liu, Y.; Wang, Q. Boosting electrochemical reaction and suppressing phase transition with a high-entropy O3-type layered oxide for sodium-ion batteries. *J. Mater. Chem. A* **2022**, *10*, 14943−14953.
(35) Ding, F.; Zhao, C.; Xiao, D.; Rong, X.; Wang, H.; Li, Y.; Yang, Y.; Lu, Y.; Hu, Y.-S. Using High-Entropy Configuration Strategy to Design Na-Ion Layered Oxide Cathodes with Superior Electrochemical Performance and Thermal Stability. *J. Am. Chem. Soc.* **2022**, *144*, 8286−8295.
(36) Yao, L.; Zou, P.; Wang, C.; Jiang, J.; Ma, L.; Tan, S.; Beyer, K. A.; Xu, F.; Hu, E.; Xin, H. L. High-Entropy and Superstructure-Stabilized Layered Oxide Cathodes for Sodium-Ion Batteries. *Adv. Energy Mater.* **2022**, *12*, No. 2201989.
(37) Anang, D. A.; Park, J.-H.; Bhange, D. S.; Cho, M. K.; Yoon, W. Y.; Chung, K. Y.; Nam, K.-W. O3-type layer-structured Na0.8[Ni1/5Fe1/5Co1/5Mn1/5Ti1/5]O2 as long life and high power cathode material for sodium-ion batteries. *Ceram. Int.* **2019**, *45*, 23164−23171.
(38) Yu, T.-Y.; Ryu, H.-H.; Han, G.; Sun, Y.-K. Understanding the Capacity Fading Mechanisms of O3-Type Na[Ni0.5Mn0.5]O2 Cathode for Sodium-Ion Batteries. *Adv. Energy Mater.* **2020**, *10*, No. 2001609.
(39) Kubota, K.; Fujitani, N.; Yoda, Y.; Kuroki, K.; Tokita, Y.; Komaba, S. Impact of Mg and Ti doping in O3 type NaNi1/2Mn1/2O2 on reversibility and phase transition during electrochemical Na intercalation. *J. Mater. Chem. A* **2021**, *9*, 12830−12844.
(40) Ryu, H.-H.; Park, N.-Y.; Noh, T.-C.; Kang, G.-C.; Maglia, F.; Kim, S.-J.; Yoon, C. S.; Sun, Y.-K. Microstrain Alleviation in High-Energy Ni-Rich NCMA Cathode for Long Battery Life. *ACS Energy Lett.* **2021**, *6*, 216−223.

https://doi.org/10.1021/acsami.3c04843
ACS Appl. Mater. Interfaces 2023, 15, 34789−34796